Princeton Plasma Physics Laboratory

PPPL- 4602

PPPL- 4602

Effect of Secondary Electron Emission on Electron Cross-Field Current in ExB Discharges

Yevgeny Raitses, Igor D. Kaganovich, Alexander Khrabrov, Dmytro Sydorenko, Nathaniel J. Fisch and Andrei Smolyakov

February, 2011

Prepared for the U.S. Department of Energy under Contract DE-AC02-09CH11466.

Princeton Plasma Physics Laboratory
Report Disclaimers

Full Legal Disclaimer

Trademark Disclaimer

PPPL Report Availability

Princeton Plasma Physics Laboratory:

http://www.pppl.gov/techreports.cfm

Office of Scientific and Technical Information (OSTI):

http://www.osti.gov/bridge

Related Links:

U.S. Department of Energy

Office of Scientific and Technical Information

Fusion Links

Effect of Secondary Electron Emission on Electron Cross-Field Current in E×B Discharges

Yevgeny Raitses, Igor D. Kaganovich, Alexander Khrabrov, Dmytro Sydorenko, Nathaniel J. Fisch, and Andrei Smolyakov

Abstract— This paper reviews and discusses recent experimental, theoretical, and numerical studies of plasma-wall interaction in a weakly collisional magnetized plasma bounded with channel walls made from different materials. A low-pressure E×B plasma discharge of the Hall thruster was used to characterize the electron current across the magnetic field and its dependence on the applied voltage and electron-induced secondary electron emission (SEE) from the channel wall. The presence of a depleted, anisotropic electron energy distribution function with beams of secondary electrons was predicted to explain the enhancement of the electron cross-field current observed in experiments. Without the SEE, the electron cross-field transport can be reduced from anomalously high to nearly classical collisional level. The suppression of SEE was achieved using an engineered carbon velvet material for the channel walls. Both theoretically and experimentally, it is shown that the electron emission from the walls can limit the maximum achievable electric field in the magnetized plasma. With non-emitting walls, the maximum electric field in the thruster can approach a fundamental limit for a quasineutral plasma.

I. Introduction

Magnetized plasmas can withstand significant steady state electric fields due to reduced mobility of charged particles across the magnetic field. Control of the electric field in such plasmas has been studied theoretically and experimentally in relation to the basic science of plasma flow in crossed electric and magnetic fields (E×B) and numerous plasma applications such as magnetically confined fusion devices, including tokamaks [1,2], magnetic mirrors [3], plasma-centrifuges [4,5], filters for isotope separation and coating applications [6], Large Area Plasma Device [7] and Hall thrusters [8,9,10].

The most common way to control the electric field in the magnetized plasma is to apply a dc bias voltage (V_b ~10-10^4 V) between two or more plasma-facing electrodes, which are electrically and magnetically insulated [2,4,7,8,9,11]. One of these electrodes can be the vacuum chamber [2,7]. With respect to the magnetic field, the electrodes are placed in such a way that their plasma-facing surfaces are intersected by different magnetic field lines (Fig. 1). There are many studies devoted to the question of how the potential gets from the biased electrode to the plasma (See, for example, in Refs. [1,11,12]). For the floating electrode, the near-wall sheath maintains equal electron and ion fluxes to the wall. When the bias voltage, V_b, is applied with respect to the plasma, the electrode can drive the current depending on the bias voltage. The sheath screens the plasma from the negative-biased electrode (cathode). For a non-emitting cathode, the potential drop across the sheath can be ~ V_b and the current is carried by ions [11]. For the positive electrode (anode), the sheath screening is much weaker. For low pressure discharges, the electron-repelling anode sheath (when the anode potential is lower than the plasma potential) has the potential drop on the order of the electron temperature, T_e, [11,13] while the potential drop of the electron-collecting anode sheath can reach the magnitude of the order of the ionization potential of the working gas [13]. Thus, for the E×B configuration shown in Fig.1, the electric potential of the plasma along the magnetic field lines, which intersect the positive electrode, is near the anode potential. With the increase of the electron emission from the negative electrode, the voltage potential drop across the cathode sheath reduces [13]. As a result, the electric potential of the plasma along the magnetic field lines, which intersect the negative electrode, can be near the cathode potential. Therefore, the electron emission from the segmented biased electrodes (Fig. 1) can be used as a valuable tool for controlling the electric field in magnetized plasmas.

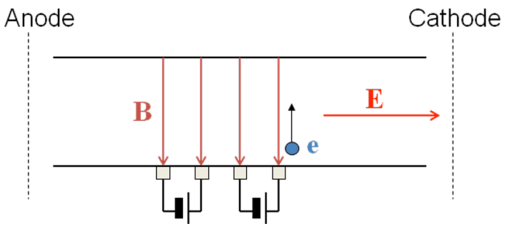

Fig. 1 Control of the electric field in E×B configuration of the Hall thruster discharge between the anode and the cathode and with biased segmented electrode [9].

The ultimate goal of the electrode biasing is to create and control the electric field in the plasma. This electric field can be used in order to, for example, accelerate the ions and generate the thrust [8-10], focus the plasma flow [8], reduce the transport phenomena [1,2,7], suppress instabilities [3,7], improve plasma confinement [4], and facilitate the mass separation [6]. The conductivity of the plasma along the field lines is stronger than the conductivity across the magnetic field. From Ohm's law, the electric field between the

Manuscript received
This work was supported by US DOE Contract No. AC02-76CH0-3073.
Y. Raitses (yraitses@pppl.gov), I. Kaganovich, A. Khrabrov and N. J. Fisch are with the Princeton Plasma Physics Laboratory, Princeton University, Princeton, NJ 08543.
D. Sydorenko is with the University of Alberta, Edmonton, AB, T6G 2G7, Canada.
A. Smolyakov is with the University of Saskatchewan, Saskatoon, Saskatchewan S7N 5E2, Canada

electrodes is inversely proportional to the cross-field conductivity. It is well known that in many practical implementations of the magnetized plasmas, the cross-field transport is governed by non-classical mechanisms [7,11,14]. These mechanisms can cause the enhancement of particle and heat transport across the magnetic field as compared to the classical collisional transport. In turn, the enhanced transport can limit the maximum achievable electric field in the magnetized plasma [10,15].

In this paper, we consider a weakly collisional plasma in applied electric and magnetic fields, with magnetized electrons and unmagnetized ions. Under such conditions, the electron cross-field current can be driven in the plasma. This current will be carried by ions and electrons. Among various physical mechanisms, which can potentially contribute to the non-classical electron cross-field transport, scattering of electrons on turbulent fluctuations of the electric field is believed to be the most common type (see, for example, Refs. [7], [14] and [15]). Resulting anomalous transport, which significantly exceeds the classical values, may exhibit both Bohm ~ $1/B$ and gyro-Bohm ~ $1/B^2$ scaling depending on the regime and experimental conditions [16]. Plasma-wall interaction can also cause the enhancement of the electron cross-field transport [10,15,17,18,19,20,21]. For example, if the magnetic field lines intersect a plasma-facing conductive wall, a short-circuit current through this wall can increase the total cross-field current (Simon's effect) [17,19,21]. Another example is the so-called near-wall conductivity induced by secondary electron emission (SEE) from the wall. This mechanism was proposed by A. I. Morozov [18] to explain anomalously high electron cross-field current in Hall thrusters. A simplified physical explanation of the near-wall conductivity is as follows. In the presence of a strong SEE from the wall, the voltage potential drop across the plasma-wall sheath decreases. The resulting enhancement of electron-wall collisions leads to the electron cross-field current carried by secondary electrons in the plasma [15,19,22,23,24]. The near-wall conductivity scales as the classical collisional transport, i.e. $1/B^2$ [18], which is also similar to the gyro-Bohm turbulent transport. The SEE effect on the electron cross-field current in a Hall thruster is the focus of this paper. The presented results are also relevant to general E×B plasma flow in various laboratory and applied configurations with electron emitting walls.

A Hall thruster is a crossed-field discharge device, which is used for spacecraft propulsion. In a conventional Hall thruster (so-called Stationary Plasma Thruster or SPT), the axial electric and radial magnetic fields are applied in an annular ceramic channel [18]. The thruster plasma is low pressure, weakly collisional (density of gas atoms, $n_a \sim 10^{12}$- 10^{13} cm^{-3}, electron plasma density $n_e \sim 10^{11}$- 10^{12} cm^{-3}) with $\rho_e \sim 0.1$ cm $< L \sim 1$ cm $<< \rho_i \sim$ 10-100 cm. Here, ρ is the Larmor radius, L is a characteristic size of the plasma, and e and i denote electrons and ions. The electric field supplies energy mainly to accelerate the ions, but some energy is also spent to heat the electrons, which diffuse across the radial magnetic field. Conventional SPT-type thrusters usually operate with xenon gas. The maximum electron temperature is $T_e \sim$ 20-50 eV [23]. This is large enough to cause strong electron-induced SEE from most ceramic materials leading to the near-wall conductivity [18].

The physics of Hall thruster has been the subject of considerable research efforts, including experimental, theoretical and numerical studies (see, for example, Refs. [18,25-34]). Because the thruster plasma is weakly collisional, kinetic effects are expected to play a key role in virtually all aspects of the thruster operation [18]. In particular, the electron energy distribution function (EEDF) is predicted to depart from the Maxwellian EEDF [18,23,26,30-33]. As a result, wall fluxes from the plasma and related processes such as the near-wall conductivity, plasma divergence, wall erosion etc can be different from predictions of existing fluid theories [23]. This is important because all these processes have direct relevance to thruster performance and lifetime [19,22,24,27].

Although the importance of kinetic effects in the thruster physics was recognized in earlier 90s [18], their quantitative description remains a critical challenge. Recent advances in this area are associated with comprehensive measurements of plasma properties in the thruster discharge [25,28,29], full particle-in-cell (PIC) simulations [30,31,32,33] and kinetic modeling [15,23,26,34] of the thruster plasma. In this paper, we review key results of these studies and analyze their implications for Hall thrusters and general E×B configurations. In this respect, the most remarkable new experimental result is the direct evidence of improved insulation properties of the magnetized plasma where SEE is suppressed. In particular, it is shown that without SEE, the plasma can withstand two-three time larger electric fields than it can do in the presence of SEE. The suppression of SEE was achieved using an engineered carbon velvet material for plasma-facing walls of the thruster channel.

The paper is organized as follows. In Section 2, we give general considerations on plasma-wall interaction in the presence of electron emission, including fluid and kinetic descriptions of the SEE effects. We also described the results of kinetic simulations. Here, we focus on electron-induced SEE from ceramic walls, but the results are relevant to a more general case of a plasma bounded by self-emitting walls, including conductive and dielectric walls. The notion of self-emitting walls implies that the electron emission is induced by plasma-wall interaction (for example, electron or ion-induced SEE or self-heating which maintains thermionic emission or field emission due to the electric field in the sheath). Section 3 describes experimental techniques used for studies of plasma-wall interactions in Hall thrusters and reviews experimental results, including the electron cross-field mobility deduced from plasma measurements for different channel wall materials with different SEE properties. Conclusions and their practical implications are summarized in Section 4.

II. Theoretical description of SEE effects on sheath and plasma properties

A. Fluid model for description of SEE effects on sheath and plasma properties

It is well-known that the electrons emitted from a surface of the floating wall into the plasma reduce the voltage potential drop in the plasma-wall sheath due to the reduction of the net

positive charge in the sheath (Fig. 2) [35]. In the case of, for example, thermionic emission, the flux of emitted electrons depends on the wall temperature and the work function of the wall material. The electron–induced SEE is a function of the energy of primary electrons from the plasma (or electron beam) and the SEE properties of the wall material. Secondary electrons emitted from a surface are commonly divided in two categories, low-energy "true" secondary electrons with energy of several electron-volts, and high-energy inelastically and elastically backscattered electrons with energy in the range from several tens of electron-volts up to the energy of incident electron [36].

In a quasineutral plasma, the electron flux to the wall, Γ_e, is balanced by the flux of ions, Γ_{ion}, and emitted secondary electrons, Γ_{SEE}. This flux balance can be expressed as

$$\Gamma_e = \frac{1}{1-\gamma(T_e)}\Gamma_{ion} \qquad (1)$$

where $\gamma(T_e) \equiv \Gamma_{SEE}/\Gamma_e$, is the averaged SEE coefficient. Fig. 2 illustrates the SEE effect on the plasma-wall sheath according to Ref. 35, under the assumption of a Maxwellian EEDF. When the flux of secondary electrons from the wall approaches the flux of primary electrons from the plasma, $\gamma(T_e) = \gamma_{cr} \approx 1$, the sheath becomes space charge saturated (SCS). Any further increase of the secondary electron flux into the plasma is restricted by a potential minimum formed near the wall surface.

Under conditions of the SCS sheath (Fig. 2), the plasma potential with respect to the wall is reduced to nearly $\Phi_w \sim T_e$, as compared to several times T_e without SEE (for example, for

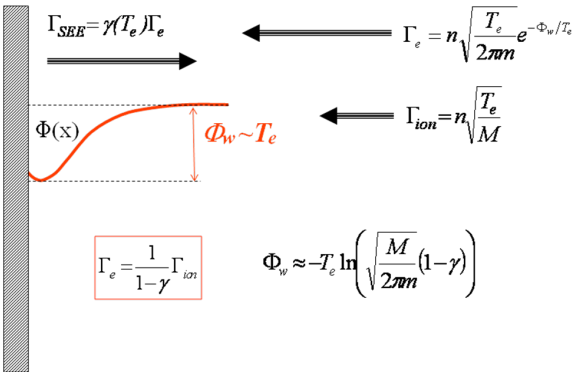

Fig. 2 Effect of the electron emission on the plasma-wall sheath (according to the fluid description of Ref. [35]). The voltage drop across the sheath reduces as the SEE coefficient approaches $\gamma_{cr} \approx 1$.

Xenon, $\Phi_w \approx 5.77\ T_e$ without SEE [37]) and the electron flux to the wall (Eq. 1) is considerably larger than the electron flux without SEE. As a result, wall acts as an extremely effective energy sink [11]:

$$q_e \approx \left(\frac{2T_e}{1-\gamma(T_e)} + e|\Phi_w|\right)\Gamma_{ion}, \qquad (2)$$

where q_e is the electron power flux density removed from the plasma. Eq. 2, accounts for the fact that only electrons with energies of $\geq e|\Phi_w|$ will reach the wall. This is without taking into account electron energy losses in the pre-sheath and the energy returned to the plasma with secondary electrons. For example, for xenon plasma, the SCS regime occurs when the SEE coefficient approaches its critical value $\gamma_{cr} = 1\text{-}8.3\cdot(m/M)^{0.5} \approx 0.983$ [35]. Here m and M are the electron mass and ion mass, respectively. For the plasma bounded with ceramic walls made from, for example, a boron nitride ceramic, the critical SEE is achieved when the electron temperature $T_e \approx 18$ eV [38]. According to the fluid models of the Hall thruster [19,22,24], because of the SCS sheath regime, the maximum electron temperature should not exceed this critical temperature.

Finally, for Hall thrusters and similar E × B discharges, the SCS sheath regime can have another important implication. According to Ref. [19,24], the effective electron-wall collision frequency in the thruster channel increases drastically when the sheath is space-charge saturated

$$\nu_{ew} \equiv \frac{\Gamma_e}{n_e H} \approx \frac{1}{n_e H}\frac{\Gamma_{ion}}{1-\gamma(T_e)}, \qquad (3)$$

where H is the distance between the channel walls or channel height. This leads to the enhancement of the electron cross-field conductivity (near-wall conductivity [18]).

B. Kinetic treatment of SEE effects on sheath and plasma properties

For collisionless and weakly collisional plasmas, where the electron mean free path, λ_{em}, is larger than the characteristic size of the plasma, the assumption of Maxwellian EEDF cannot be justified. Indeed, energetic electrons should quickly escape from the plasma to the wall. Depending on their energy at the wall, these electrons can be either lost due to a wall recombination with ions or liberate SEE electrons from the wall. In the absence of sufficient electron-electron collisions in the plasma, there is no obvious mechanism to maintain the Maxwellian EEDF. Under such conditions, the resulting EEDV is depleted at high energies due to wall losses. Because $\lambda_m > H$, the electron losses to the walls can be hundreds of times smaller than the losses predicted by the fluid theories (Fig. 2 and Eqs. 1-3) [23]. A similar depletion of EVDF at high energies was also reported for other kinds of low pressure discharges [39, 40].

Another important aspect of low collisionality in low pressure plasmas is that electron-atom and electron-ion collisions are not frequent enough to isotropize the electron velocity distribution function (EVDF). Therefore, the depletion of energetic electrons in the velocity phase space is expected to occur mainly in the direction towards the wall. As a result, the EVDF can become anisotropic [23,30].

In Refs. [30-32], a full 1-D 3-V particle-in-cell code was used to study the EVDF and SEE effects in the weakly collisional magnetized plasma of the Hall thruster (H = 2.5- 3 cm, $n_e \sim 10^{11}$-10^{12} cm^{-3}, $n_a \sim 10^{12}$-10^{13} cm^{-3}, and $E \sim 10^2$ V/cm, $B \sim 10^2$ Gauss). Illustrative results of PIC simulations using this code for the EVDF with and without SEE are shown in Fig. 3. Compared to previous simulations [23,30-32] , these

results were obtained using improved analytical approximations for differential cross sections for scattering of electrons in electron-neutral elastic collisions described in Appendix 1. The simulations considered the electric field in the range of 50-200 V/cm and predicted the effective electron temperatures of 20-40 eV and 10-12 eV in the direction parallel and perpendicular to the wall, respectively. In addition to numerical simulations, Ref. [23] developed analytical expressions to characterize the effects of low plasma collisionality on the plasma-wall interaction. The flux of plasma electrons to the wall is predicted to be $h/2\lambda_m$ times smaller as compared to Γ_e for the Maxwellian EVDF. This factor accounts for the depleted loss cone of the velocity space in the direction towards the wall.

Note that we use here the term loss cone to describe the area in the velocity phase space which contains particles with the energy of motion normal to the walls sufficient to penetrate through the potential barrier of the sheath [30].

Because of the reduced electron flux to the wall, the plasma potential with respect to the wall is also reduced as compared to the plasma case with the Maxwellian electron energy distribution function $\sim \Phi_w - T_e \ln(\lambda_m / H)$. Here, for the plasma with non-Maxwellian EVDF shown in Fig. 3, T_e is the effective electron temperature [23,30]. For example, for the Hall thruster, PIC simulations predicted a plasma potential of 20-28 V, $\Phi_w \sim T_e$ [23]. This is significantly smaller than the plasma potential estimated for the Maxwellian EEDF and xenon without electron emission, $\Phi_w \approx 5.77\ T_e$ [37].

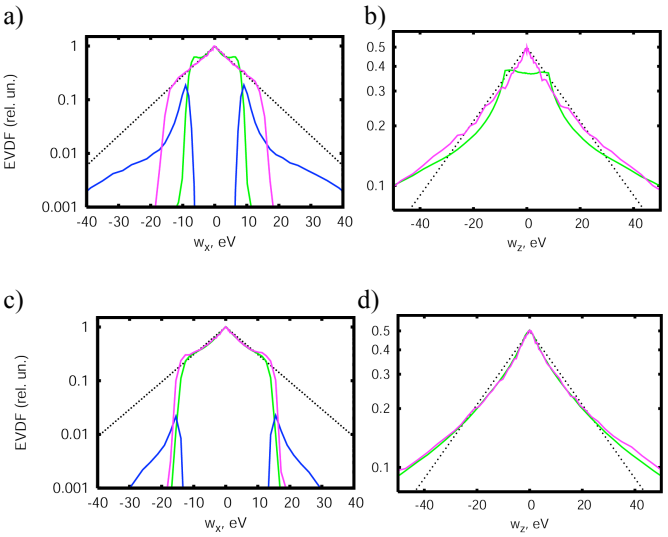

Fig. 3 Results of Particle-in-Cell simulations for E×B plasma slab bounded between two walls. The simulations were conducted using a full 1-D 3-V PIC code [23,30-32]. The electron velocity distribution function (EVDF) along and across the magnetic field (B = 100 Gauss): a) and b) for E = 200 V/cm, and c) and d) for E = 100 V/cm. In addition, the following input parameters were used for these simulations: the neutral density of $1 \cdot 10^{13}$ cm^{-3}, the effective anomalous collision frequency of $2.8 \cdot 10^6$ s^{-1} and the B-field of 100 Gauss. The simulated plasma density is $2.7 \cdot 10^{11}$ cm^{-3} for a) and b) and $4.3 \cdot 10^{11}$ cm^{-3} for c) and d). The EVDF is compared for plasmas with and without secondary electron emission: a) and c) in the X-direction normal to the wall and parallel to the magnetic field, and b) and d) in the Z-direction parallel to the wall and the electric field. The EVDF's of the bulk plasma with and without SEE are shown with green and magenta lines, respectively. The EVDF of counterstreaming SEE beams is shown with blue lines. For comparison, the Maxwellian EVDF is shown for each direction with dashed black lines (for E=200 V/cm, T_{ex} = 8.1 eV and T_{ez} = 25.2 eV, and for E = 100 V/cm, T_{ex} = 8.5 eV and T_{ez} = 23 eV,). The main results are: 1) the EVDF over velocity normal the wall is depleted at high energy tail due to loss of fast electrons at the walls; 2) EVDF over the velocity parallel to the wall is not depleted due to rare collisions which scatter electrons to the loss cone; 3) with SEE, there are counterstreaming beams of secondary electrons propagating between two opposite walls; 4) strong SEE effects occur when the beam energy is large enough to sustain the counterstreaming beams. The latter requires a strong electric field in the plasma (≥ 200 V/cm).

Because the EVDF is not depleted in the direction of the electric field, parallel to the wall, (Figs. 3b and 3d), high energy electrons with energy above the plasma potential Φ_w are preserved in the plasma. The flux of these electrons to the wall is controlled by rare collisions with heavy particles (for the thruster plasma, loss cone is formed mainly by collisions with atoms) [23]. When there is no SEE (no backscattering and no true secondary electrons), the plasma electrons will be lost due to recombination at the wall. Fig. 3a (magenta curve) shows the EVDF for such electron-absorbing wall. In the presence of SEE from the wall (Fig. 3 green curves for bulk electrons), secondary electrons are accelerated in the sheath towards the plasma and form the beam (Figs. 3a and 3 c, blue curves) [30]. According to PIC simulations [30,31], the SEE beam from one wall can reach the opposite wall without being strongly affected by collisions with the other particles in the plasma or various plasma instabilities such as two-stream instability between beam of secondary electrons and plasma electrons. This situation with SEE beams unaffected by two-stream instability is similar to other low pressure magnetized plasma such as in the expansion tank of the magnetic mirror [41] and dc magnetron discharges.

Consider counterstreaming beams of secondary electrons between two opposite walls with symmetrical sheaths (Fig. 4). After gaining the energy due to the acceleration in the sheath at one wall, the beam electrons lose their kinetic energy while crossing the sheath at the opposite walls. If electron incident energy is low (< 5 eV), there is a probability for electron backscattering to occur [19,30,36]. However, the SEE due to backscattering process from metals and ceramics is always smaller than $\gamma_{cr} \approx 1$ [19,38]. A different situation can take place for the E×B configurations such as shown in Fig. 5. Here, the beam electrons gain additional energy due to the E×B motion. The energy of the beam electron at the moment of its collision

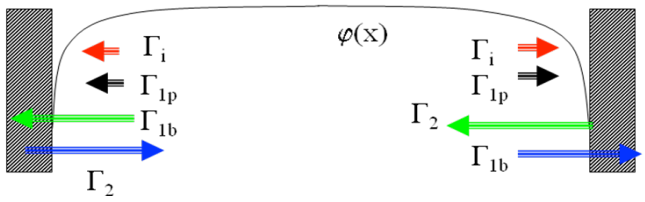

Fig. 4 Plasma-wall interaction in a weakly collisional magnetized plasma bounded between two emitting walls [23,30,34,42,43]. Γ_i is the ion flux from the plasma to the wall. Γ_{1p} is the flux of plasma electrons to the walls scattered by collisions with neutral and plasma particles. Γ_2 is the beam of secondary electrons departing from the wall. Γ_{1b} is the beam of secondary electrons arriving to one wall from the opposite walls. The plasma potential profile between the walls is also shown.

with the wall is [42]

$$\varepsilon_B = mV_{dr}^2(1-\cos\varphi), \quad (4)$$

where $V_{dr}=E/B$ is the drift velocity in crossed electric and magnetic fields, and $\varphi = \omega_{ce}\tau$ is the final phase of cyclotron rotation before the electron collides with the wall. Here, $\omega_{ce} = eB/m$ is the electron gyrofrequency and τ is the electron time of flight between the wall.

Note that, the maximum of the additional electron energy on a scale of gyroradius (Fig. 5) is

$$\varepsilon_{B\max} = 2eE\rho_e. \quad (5)$$

If this energy is insufficient to induce a strong SEE, counter-streaming beams of emitted electrons will have a weak effect on the plasma. Fig. 3 shows the simulated results for E = 100 V/cm and 200 V/cm. In addition, Table 1 summarizes the SEE yields for plasma and beam electrons. With the increase of the electric field, the beam-induced SEE, γ_b, also increases. For E = 200 V/cm and $\rho_e \approx 0.15$ cm, the maximum possible beam energy (Eq. 5) $\varepsilon_{Bmax} \approx 60$ eV. According to Eq. 4 and Ref. 42, this is large enough to ensure that beams induce $\gamma \approx \gamma_{cr}$ from a Boron Nitride ceramic [38] – the material of the thruster channel walls. A detailed analysis of the simulated results for the EVDF in the thruster plasma and its dependence on the input parameters, including the electric field, effective frequency of turbulent collisions, and the channel height is described elsewhere [23,30-32, 42-43].

Table 1 The effect of the electric field on the near-wall conductivity induced by SEE beams. γ_p , γ_b, are partial SEE coefficients due to plasma and beam electrons, respectively. γ_T is the total SEE coefficient [42].

E, V/cm	γ_p	γ_b	γ_T	$J_{NW}/J_{e\perp}$
100	1.5	0.69	0.83	≤ 0.05
140	1.65	0.82	0.9	0.25
200	1.54	0.97	0.978	0.64

Note that in the case of symmetrical sheaths on both walls and strong SEE from these walls, the contribution of the arriving and departing beams to the total current balance on each wall is canceled [23,34]. Under such conditions, the sheath potential between the floating emissive wall and the plasma is determined by the balance between the ion flux and the electron flux from the plasma (loss cone) [23]. This is equivalent to the case of the plasma-wall sheath in the absence of the electron emission.

C. Kinetic treatment of SEE effects on SEE-induced electron cross-field current

For the Hall thruster and similar E×B configurations, the counterstreaming SEE beams can induce the enhancement of the electron cross-field current (near-wall conductivity,[18]) [23,30,43]. This occurs because a secondary electron during one pass from one wall to the opposite wall moves across the magnetic field towards the anode by the distance of the order of the electron gyroradius (Fig. 5). According to Refs. [23, 43], the axial electron current density due to the beams of SEE electrons (near-wall conductivity) is

$$J_{NW} \propto \frac{1}{H}\frac{\gamma_p}{1-\gamma_b} n_e \sqrt{\frac{T_{e\perp}}{M_i}} \frac{E_\perp}{B^2}, \quad (6)$$

where γ_p and γ_b are the partial SEE coefficients for plasma and beam electrons, respectively. Because the near-wall conductivity is carried by the SEE beams, its contribution to the electron cross-field current increases with the beam energy (Eqs. 4 and 5) and becomes the dominant mechanism of cross-field current in the thruster when γ_b approaches 1 (Table 1).

According to Eqs. 4 and 5, the beam energy is determined by the strength of the electric field, which depends on the discharge voltage, V_d. Changes of the magnetic field, which can affect the electric field, can also be accompanied with changes of the maximum beam energy (Eq. 5). In addition, the distance between the channel walls, can have a non-monotonic effect on the final phase of cyclotron rotation, φ, [42] and thereby, on the incident energy and incident angle of beam electrons at the wall. Simulations predict that with all input parameters the same, the reduction of the electric field causes an abrupt reduction of the near-wall conductivity (Table 1).

When the density of neutral atoms near the wall has a local peak due to, for example, recombination at the wall or outgasing from the wall during the plasma discharge, collisions of secondary electrons with atoms can additionally enhance the near-wall conductivity [44]. Moreover, a high frequency sheath instability, which is predicted to occur in the SCS regime, may also contribute to the enhancement of the electron cross-field transport [33]. This instability occurs due to a negative differential resistance of the sheath near the

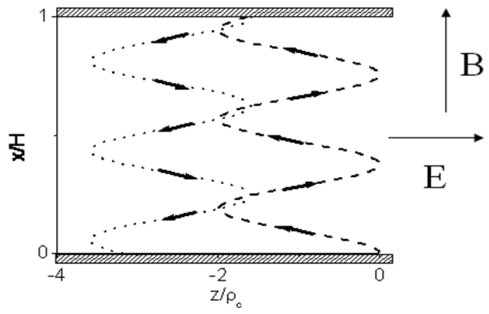

Fig. 5 Schematic illustration of the near-wall conductivity in crossed electric and magnetic field due to the counterstreaming beams of secondary electrons [23].

emitting wall [32,33].

Note that there are a number of other factors which can alter the SEE effect on the plasma-wall interaction and the near-wall conductivity. For example, cylindrical geometry and a two-dimensional topology of the magnetic field, including oblique magnetic field with respect to the emitting wall can alter the SEE [15,45] asymmetrical sheath conditions on the opposite channel walls [33]. This may change the total current balance at the walls. In the next section, we compare wall material effects on the thruster operation with the same

magnetic field topology and the channel geometry.

III. Experimental demonstration of SEE effects on plasma properties and the electron cross-field current

A. Materials for non-emitting (absorbing) and emitting walls

There is a reliable experimental evidence that the Hall thruster operation is very sensitive to the wall material of the thruster channel [10,19,46,47,48]. Conventional Hall thrusters use a boron nitride ceramic as the channel wall material [18,19,47]. Several studies pointed to the existence of a correlation between the discharge current and SEE properties of the ceramic wall materials [19,46,47]. In particular, for constant discharge voltage and magnetic field, larger values of the discharge current were measured for ceramic materials with lower values of the energy threshold for the SCS. However, for the most of ceramic materials applicable for thruster applications, this energy threshold is in the range between 30-40 eV [38]. This is comparable with measurement uncertainties of the electron temperature and the plasma potential for the probe diagnostics used in these studies [28,48]. Therefore, it is not so obvious that the observed differences in the thruster operation with different ceramic wall materials of the thruster channel can be attributed to differences in the SEE properties of these materials.

Note that during the thruster operation, surface properties of the ceramic walls, including the SEE may be affected by outgasing [49], physical and chemical sputtering and deposition of various coatings and high temperature (~ 1000 C). There is no published data on SEE yield from ceramic materials after and during their exposure to the plasma. This can also complicate a validation of theoretical predictions of the SEE effects in the thruster discharge.

In a number of thruster studies, the channel walls were made from metal and graphite materials [10,19,20,29,46-48,50,51]. For typical electron temperatures in the thruster discharge (20-50 eV), these materials have much lower SEE than ceramic materials. For example, for graphite-type materials, even the maximum SEE yield (at the energy of primary electrons of 300 eV) may not reach the critical yield for the SCS sheath with Xenon gas ($\gamma_{cr} \approx 0.983$). With a smaller SEE, the electron cross-field current is expected to be smaller (Table. 1 and Eq. 4). However, the short-circuit current through the conductive wall made from metal or graphite materials can increase the discharge current [10,19,20,47].

In the absence of electron emission from the conductive wall, the short-circuit current is determined by the ion flux to the wall and the ion-collecting area [19,20]. For a typical SPT-type Hall thruster, the length of the annular channel measured between the anode and the channel exit can be several centimeters. When the channel walls are made entirely from metal or graphite materials, the resulting discharge current can be larger than the discharge current for the thruster with ceramic walls [19,47]. This is partially because the ion flux from the plasma is collected by the entire channel. The reduction of the ion collecting area can reduce the short-circuit current [19,20]. All critical plasma parameters of the thruster discharge, including the electric field and the electron temperature, reach their local maxima within a ~ 0.5-1 cm region from the channel exit inside the thruster channel [10,28,52,53]. Therefore, it was sufficient to place short-length segments made from low SEE and low sputtering conductive materials in this region in order to affect the thruster plasma without a large short-circuit current [10,20,29, 50,51].

Fig. 6 shows a 2 kW laboratory Hall thruster with two approximately 1cm length conductive segments placed on inner and outer walls of the boron nitride ceramic channel [29,50]. The channel outer diameter is 12 cm, H = 2.5 cm and the channel length, L, is 4.6 cm. Because both segments can be floating or biased, we shall refer to them as segmented electrodes. These segmented electrodes were made from graphite velvet material [50]. Sputter-resistance of this engineered metamaterial is exceptionally good, particularly, with respect to the backflow of contamination. This is because ions strike the velvet at grazing incidence and sputtered particles get trapped in the velvet texture (Fig. 6c). An important feature of carbon velvet is that because of interfiber cavities with a large aspect ratio of ~10^2 it is expected to suppress both ion-induced and electron-induced secondary electron emissions from the electrode [29]. In addition, the

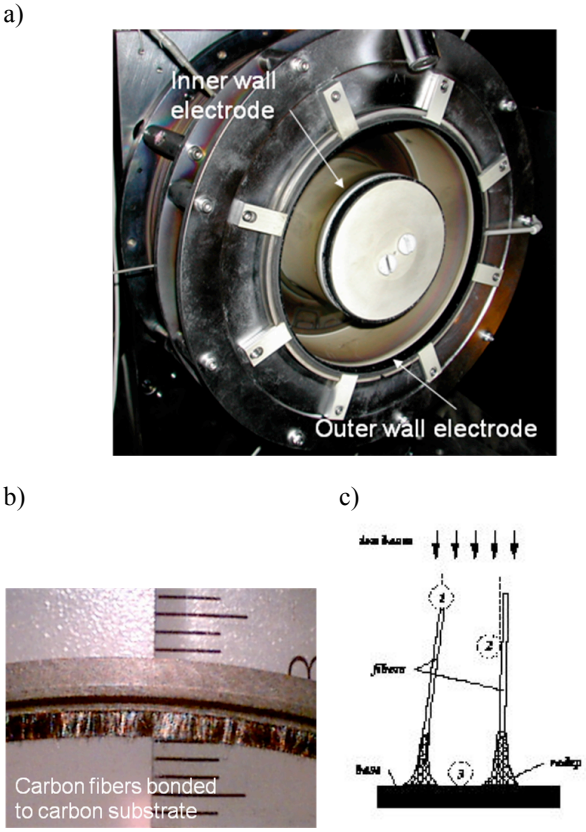

Fig. 6. A 2 kW segmented electrode Hall thruster: a) narrow segmented electrodes are placed at the exit of the 12 outer diameter thruster channel made from a boron nitride ceramic material; b) the segmented electrodes are made from sputter-resistant carbon-velvet material to suppress the SEE [50]; (c) schematic of the velvet material (Courtesy of Energy Science Laboratories, Inc., http://www.esli.com). In the thruster operation, the electrodes can be floating or biased with respect to the cathode.

graphite velvet allows to minimize the backflow of atoms resulted from recombination at the wall. Thus, the use of graphite velvet material offers a unique opportunity to achieve the operation of the Hall thruster without the SEE-induced near-wall conductivity.

B. *Remarks on probe measurement procedures*

In the described experiments, plasma properties, including plasma potential and electron temperature, were measured using various movable and stationary electrostatic probe techniques, including emissive probes and biased collecting probes. A detail description of the probes, measurement procedures used in these experiments, the analysis of measurement uncertainties and probe-induced perturbations of the plasma are given in Refs. [28,54,55]. The electric field was

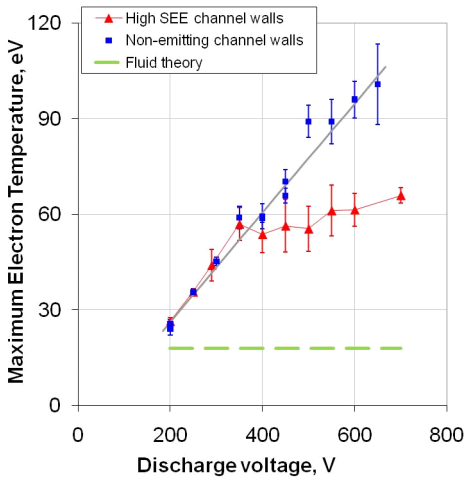

Fig. 8 A comparison of the measured maximum electron temperature as a function of the discharge voltage for high SEE boron nitride ceramic walls and non-emitting carbon velvet walls (floating segmented electrodes on outer and inner channel walls, Fig. 6) [29]. The discharge voltage controls Joule heating of electrodes. The dashed green curve corresponds to the maximum temperature in the channel estimated according to the fluid theory of Ref. [35]. The magnetic field and the gas flow rate are constant for all discharge voltage regimes.

energy above some threshold in this direction is larger than the corresponding flux along the magnetic field lines. The ratio of these fluxes is about the square root of the ratio of electron temperatures parallel and normal to the walls if the threshold is below the plasma potential with respect to the wall (the energy where the depletion of the electron distribution over the velocities normal to the wall begins). In our PIC simulations (Fig. 3 and Refs. [30-32]), the ratio of temperatures was usually about 3. Hence, the ratio of fluxes is about 1.7 for electron energies below the plasma potential with respect to the wall. If the aforementioned threshold is above the plasma potential, this ratio can be much larger. For example, for the case with the electric field E = 140 V/cm (Table 1), the flux ratio is about 2.5 times. Thus, in our probe measurements, the contribution of the electron flux parallel to the walls is predicted to be dominant over the electron flux along the magnetic field lines. It may imply that the temperature deduced from these measurements is approximately the effective electron temperature perpendicular to the magnetic field, T_{ez}. This is relevant to all thruster regimes in which the electron E×B drift velocity, V_{dr}, is sufficiently smaller than the electron thermal velocity, V_{th}. As it is shown in the next section of this paper, there are high discharge voltage regimes of the thruster with non emitting walls for which $V_{dr} \geq V_{th}$.

C. *Measurements of the SEE effects on sheath and plasma properties*

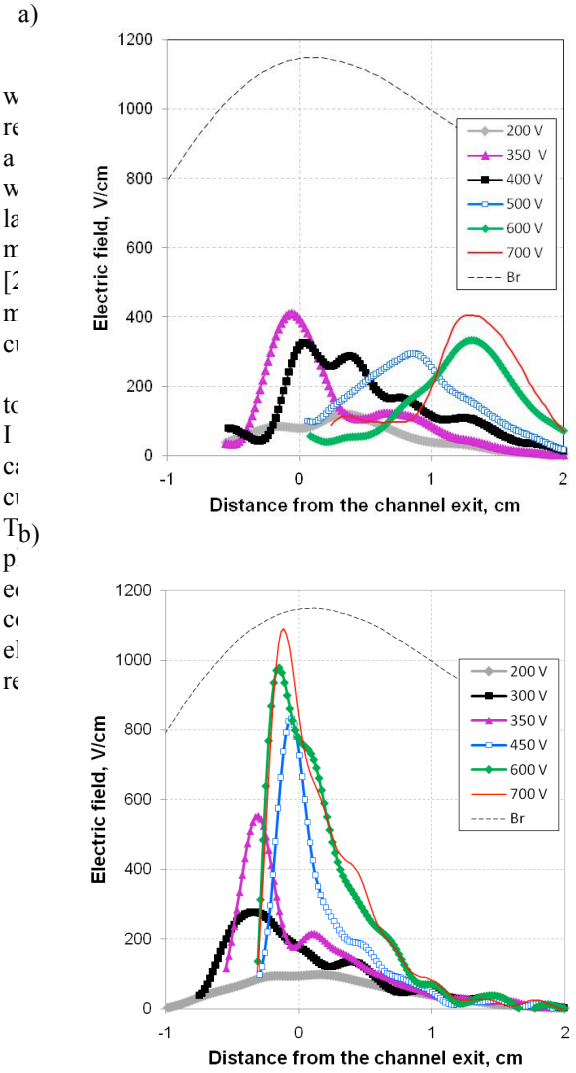

Fig. 9 The electric field along the thruster channel median obtained for the high SEE channel made from boron nitride ceramic (a) and for segmented thruster with non-emitting floating walls made from carbon velvet material, Fig. 6, (b). The anode position inside the thruster channel is at the distance of – 4.6 cm from the channel exit. The magnetic field and the gas flow rate are constant for all discharge voltage regimes. The profile of the radial magnetic field is also shown with the maximum magnetic field, B_{rmax} = 115 Gauss. The electric field was obtained by differentiating the measured plasma potential distribution along the channel median.

Note that for high SEE channel case (top figure), fast movable probe, which was used for plasma potential measurements, induced strong plasma perturbations at high discharge voltages [28]. For the probe measurements inside the channel, where probe-induced perturbations of the plasma were particularly strong, the electric field is not shown.

discharge. For both channel wall materials, where a linear increase of the maximum temperature with the discharge voltage exists, the wall material effects are minor in these regimes. The temperature saturation observed for the ceramic channel case, was attributed to the SEE effect [28].

The fact that the electron temperature at saturation is higher than predicted by fluid theories [10,19,24,56] suggests that understanding the Hall thruster plasma in detail requires a kinetic treatment [23,30,43]. In particular, it may suggest the presence of a depleted, anisotropic electron energy distribution function with beams of secondary electrons leading to the near-wall conductivity [23,30-32,42,43]. This could explain the increase of the electron cross-field current with the discharge voltage observed for the high SEE case (Fig. 7).

Fig. 9 demonstrates the axial electric field distribution measured for high SEE and non-emitting channel wall cases. The electric field was obtained by differentiating the measured plasma potential distribution along the channel median [28]. The most significant differences between these two cases are observed at high discharge voltages: 1) With non-emitting walls, the electric field can be 2-3 times larger than with high SEE walls. In the later case, the increase of the discharge voltage causes the potential drop to occur along the longer region. This region extends inside the ceramic channel and in the plasma plume [28,37]; 2) With high SEE walls, the maximum electric field shifts to the near-plume region away from the channel (Fig. 9a). This is not the case for the non-emitting walls (Fig. 9b). Here, even at high discharge voltages, the maximum electric field remains inside the channel in the region of a strong magnetic field.

For high SEE walls, the observed changes of the electric field distribution with the discharge voltage (Fig. 9a) can be explained by the enhancement of the electron cross-field current inside the high SEE channel. The near-wall conductivity seems to be the most likely mechanism responsible for this enhancement. With a constant discharge voltage, the SEE-induced near wall conductivity causes a larger fraction of the voltage potential drop to be placed outside the channel [10,28,37,48,56]. Here, the maximum electric field reaches its local maximum.

For high discharge voltage operation without SEE, the electric field inside the channel can be strong (~ 10^3 V/cm, at V_d > 600 V Fig. 9b), while with SEE, the maximum electric field inside the channel does not exceed ~ 100 V/cm at V_d >400 V (Fig. 9a). For E =100 V/cm and ρ_e =0.15 cm, $\varepsilon_{Bmax} \approx$ 30 eV (Eq. 5) is just enough to get $\gamma(\varepsilon) \approx 1$ from Boron Nitride [38]. According to Ref. 42, $\varphi \neq \pi/2$ (Eq. 4). Thus, the beam energy at E = 100 V/cm seems to be not enough to sustain strong beams of secondary electrons Among possible explanations of this discrepancy between predictions of PIC simulations and the experiment, we can mention probe–induced perturbations of the plasma inside the channel [28,54], limitations of one-dimensional code and possible time-dependent processes in the thruster (e.g. oscillations of the electric field [25,33]), which were not captured by steady-state measurements in the described experiments.

Without specifying the exact mechanism of the electron transport, we shall compare the electron cross-field mobility, $\mu_\perp = ev_e / m_e\omega_{ec}^2$ for high SEE and non-emitting wall cases. The mobility can be deduced by substituting measured plasma parameters into one-dimensional Ohm's law,

$$v_{ez} = \mu_\perp \left[E - (1/en_e)d(n_eT_e)/dz\right] \quad (7)$$

The electron velocity was estimated using the measured plasma and discharge parameters, $v_{ez} = I_e/en_eA$, where A is the plasma cross-section (in the channel or in the plume deduced from measured plume divergence angle). The mobility varies along the thruster channel because of non-uniform magnetic field and variations of the electron collision frequency, v_e. Fig. 10 compares the experimental electron mobility, which was obtained at the local maximum of the electric field, as a function of the discharge voltage. In addition, the classical mobility estimated for electron-atom collisions is also shown in Fig. 10. The atom density was assumed to be $5\cdot10^{12}$ cm^{-3}, which is typical for Hall thrusters. For each discharge voltage, the electron temperature measured for the thruster with non-emitting walls was used for the estimation of the classical mobility. For the thruster with high SEE walls, the temperature saturates above 400 V. In any case, for both wall materials, the experimental mobility appears to be larger than classical.

When SEE has no effect on the thruster plasma (below the voltage threshold of 400 V), the mobility trends are not so

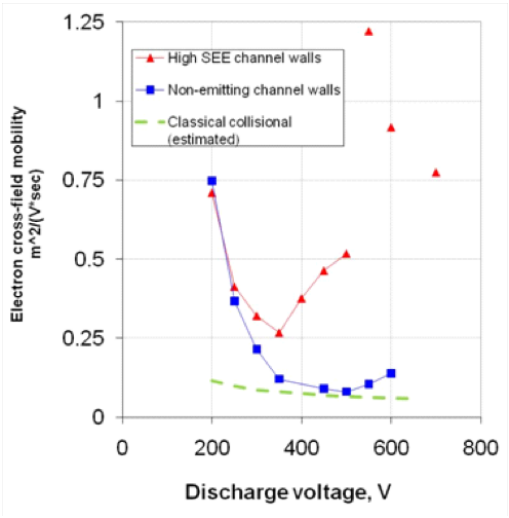

Fig. 10 A comparison of the electron cross-field mobility with the classical mobility for high SEE boron nitride walls and non-emitting carbon velvet walls (floating segmented electrodes on outer and inner walls of the channel, Fig. 6). The experimental mobility was deduced from measurements at the local maximum of the electric field. The classical mobility (dashed green curve) was estimated under the assumption of dominant electron-atom collisions at $n_a = 5\cdot10^{12}$ cm^{-3} and using T_e measured for the thruster with non-emitting walls.

sensitive to the wall material. In the absence of the near-wall conductivity, the enhanced electron conductivity may be caused by anomalous fluctuation-induced mechanism. It is indeed surprising that for both wall material cases, the mobility tends to decrease as the discharge voltage (and the electric field) increase to the discharge voltage of 350 V. This mobility reduction with the discharge voltage is not understood at the moment. A shear-based mechanism of the

reduction of the electron transport in the Hall thruster discharge has been proposed by Cappelli *et. al* [57] and developed by Scharfe *et. al* [58] within semi-empirical analysis and without identification of the mode(s) responsible for anomalous transport.

The E × B shear could possibly be responsible for the reduction of the mobility with the discharge voltage observed in the present study (Fig. 10). The shear of the E×B velocity along the channel becomes larger with the increase of the maximum electric field at a constant magnetic field (Fig. 9). This is particularly relevant for the thruster with non-emitting walls. For this thruster, a simplified calculation of the shearing frequency, $d(E_z/B_r)/dz$, suggests that it increases from 0.15 ns^{-1} at 200 V to 5-8 ns^{-1} at 600 V. With high SEE walls, the shearing frequency reaches its maximum of about 1 ns^{-1} at 350-400 V and then drops at higher discharge voltages. Large shear of the electric field may affect the dynamics of instabilities, which were predicted and some of which were measured for conventional Hall thrusters at moderate discharge voltage [18,25,59,60,61]. Furthermore, large shear of the electric field, which may exist in the thruster with non-emitting walls, may lead to the occurrence of specific kinetic regimes [32, 43].

At high discharge voltages, the mobility increases for high SEE walls, but continues to drop for low SEE walls. The former result can be attributed to the SEE-induced near-wall conductivity. Within the accuracy of the probe measurements [28], the electron cross-field transport in the channel with low SEE walls is suppressed to almost classical level. Apparently with non-emitting walls, it is possible to significantly improve insulation properties of the magnetized plasma at high discharge voltages as compared to the plasma bounded with high SEE walls. With such improved insulation, the maximum electric field measured at > 600 V (~ 10^3 V/cm) is just a few times below a fundamental limit for a quasineutral plasma, $E \sim T_e/\lambda_D$ (for $T_e \sim 100$ eV and $n_e \sim 10^{11}$ cm^{-3}), where λ_D is the Debye length. Moreover, in these regimes, the E×B rotation of electrons becomes supersonic (for example, at V_d =600 V, the ratio of the drift to thermal electron velocities at the placement of the local maximum of the electric field along the thruster channel is $V_{dr}^{max}/V_{th}^{max} > 2$). This may lead to kinetic effects on the plasma potential distribution due to increased centrifugal forces on electrons [62].

IV. Concluding remarks

The purpose of this work was to review recent experimental, theoretical and numerical studies of plasma-wall interaction in Hall thrusters and discuss their implications for control of the electric field in E×B discharges. The presence of a depleted, anisotropic electron energy distribution function with beams of secondary electrons emitted from the thruster channel walls was predicted to explain the enhancement of the electron cross-field current observed in experiments. These results support the existence of the SEE-induced near-wall conductivity in the conventional Hall thruster with high SEE ceramic walls (SPT-type) [18].

The contribution of the near-wall conductivity to the electron cross-field current increases with the electric field. This implies that the electron emission from the walls can limit the maximum achievable electric field in the magnetized thruster plasma. It is shown that without SEE, the electron cross-filed transport reduces with the discharge voltage from anomalously high to nearly classical collisional level. This reduction may be associated with shear of the electric field [57,58]. For the considered E × B configuration of the thruster, shear of the electric field can be exceptionally large when the electron emission from the wall is suppressed. Under such conditions, the magnetized thruster plasma can withstand much stronger electric fields than with emitting walls. Overall, at high discharge voltages, the thruster discharge unaltered by SEE can approach new regimes with significant electric field, pressure gradients and supersonically rotating electrons. These high magnetic insulation regimes of the E × B thruster discharge require future kinetic studies.

To conclude, for laboratory magnetized plasmas, the use of non-emitting walls is essential in order to strengthen insulation properties of such plasmas. This is particularly relevant to plasma applications for which control of the electric field is implemented with biased electrodes. Similar to this work, the suppression of SEE from, for example, the plasma facing wall between the biased electrodes, can be achieved using engineered materials such as carbon velvet [29,50]. For practical implementation of non-emitting walls, it is also important that this material is sputter-resistant. The presented results and materials can be relevant to various plasma applications, which require the suppression of SEE from the plasma-facing wall.

Acknowledgement

The authors wish to thank Drs. David Staack, Leonid Dorf and Artem Smirnov and for fruitful discussions of the experimental results. The authors are also grateful to Dr. Dr. Timothy R. Knowles of Energy Science Laboratory, Inc. for useful discussions on carbon-velvet material and its properties. This work was supported by the US DOE and AFOSR.

References

[1] V. A. Rozhansky, A. A. Ushakov and S. P. Voskboynikov, " Electric fields and currents in front of a biased electrode (flush mounted probe) and the I-V characteristics of the electrode for various mechanisms of transverse conductivity", Nucl. Fusion, vol. 39, no 5, pp 613-628, 1999.

[2] S. J. Zweben *et al.,* "Local scrape-off layer control using biased electrodes in NSTX", Plasma Phys. Control. Fusion, vol. 51, pp. 105012-36, 2009.

[3] D. D. Ryutov, "Mirror devices" Plasma Devices and Operation, vol. 1, no 1, pp. 79-96, 1990.

[4] R. F. Ellis *et al.,* "Steady supersonically rotating plasmas in the Maryland Centrifugal Experiment", Phys. Plasmas, vol. 12, pp. 055704-7, 2005.

[5] A. J. Fetterman and N. J. Fisch, "Alpha Channeling in Rotating Plasmas", Phys. Rev. Lett., vol. 101, 20500, 2008; A. J. Fetterman and N. J. Fisch, Wave-driven countercurrent

plasma centrifuge, Plasma Sources Sci. Technol., vol. 18, 045003, 2009.
[6] M. Krishnan, M. Geva and J. L. Hisrhfeld, "Plasma centrifuge", Phys. Rev. Lett., vol. 46, no 1, pp. 36-38, Jan. 1981.
[7] T. A. Carter and J.E. Maggs, "Modifications of turbulence and turbulent transport associated with a bias-induced confinement transition in the Large Plasma Device", Phys. Plasmas, vol. 16, pp. 012304-10, 2009.
[8] Y. Raitses, L. A. Dorf, A. A. Litvak, and N. J. Fisch, "Plume reduction in segmented electrode Hall thruster," J. Appl. Phys., vol. 88, no. 3, pp. 1263–1270, 2000; N. J. Fisch, Y. Raitses, L. A. Dorf, and A. A. Litvak, "Variable operation of Hall thruster with multiple segmented electrodes," J. Appl. Phys., vol. 89, no. 4, pp. 2040–2046, 2001.
[9] A. Fruchtman and N. J. Fisch, "Variational principle for optimal accelerated neutralized flow," Phys. Plasmas, vol. 8, no. 1, pp. 56–58, Jan. 2001; A. Fruchtman, N. J. Fisch, and Y. Raitses, "Control of the electric-field profile in the Hall thruster," Phys. Plasmas, vol. 8, no. 3, pp. 1048–1056, 2001.
[10] Y. Raitses, M. Keidar, D. Staack, and N. J. Fisch, "Effects of segmented electrodes in Hall current plasma thrusters," J. Appl. Phys., vol. 92, no. 9, pp. 4906–4911, 2002.
[11] P. C. Stangeby, The Plasma Boundary of Magnetic Fusion Devices, Plasma Physics Series (IOP, Bristol, 2000).
[12] N. Hershkowitz, "How does the potential get from A to B in a plasma?", IEEE Trans. Plasma Sci., vol. 22 , no.1, pp. 11-21, 1994.
[13] Yuri P. Raizer, Gas-Discharge Physics (Springer) 2001.
[14] G. S. Janes and R. S. Lowder, "Anomalous electron diffusion and ion acceleration in a low-density plasma," Phys. Fluids, vol. 9, no. 6, pp. 1115–1123, 1966.
[15] M. Keidar, I.I. Beilis, "Electron transport phenomena in plasma devices with E×B drift, IEEE Trans. Plasma Sci., vol. 34, no. 3, pp. 804-814, 2006.
[16] G. R. Tynan, A. Fujisawa , G. McKee, "A review of experimental drift turbulence studies", Plasma Phys. Control. Fusion, vol. 51, no11, 113001, 2009.
[17] A. Simon, "Ambipolar diffusion in a magnetic field", Phys. Rev., vol. 98, no. 2, 317-318, 1955.
[18] A. I. Morozov and V. V. Savelyev, Review of Plasma Physics, vol. 21, B. B. Kadomtsev and V. D. Shafranov, Eds. New York: Consultants Bureau, 2000, p. 203.
[19] S. Barral, K. Makowski, Z. Peradzynski, N. Gascon, N., and M. Dudeck, "Wall material effects in stationary plasma thrusters II. Near-wall and in-wall conductivity," Phys. Plasmas, vol. 10, no. 10, pp. 4137–4152, Oct. 2003.
[20] D. Staack, Y. Raitses, and N. J. Fisch, "Control of acceleration region in Hall thrusters" , in Proceedings of the 28th International Electric Propulsion Conference (Electric Rocket Propulsion Society, Cleveland, OH, 2003) IEPC paper 03-0273, Toulouse, France, March 2003.
[21] A. Fruchtman, "Ambipolar and nonambipolar cross-field diffusions", Plasma Sources Sci. Technol., vol. 18, pp. 025033-16, 2009.
[22] E. Ahedo, J. M. Gallardo, and M. Martinez-Sanchez, "Effects of the radial plasma-wall interaction on the Hall thruster discharge," Phys. Plasmas, vol. 10, pp. 3397–3409, 2003.
[23] I. Kaganovich, Y. Raitses, D. Sydorenko, and A. Smolyakov, "Kinetic effects in a Hall thruster discharge," Phys. Plasmas, vol. 14, no. 5, p. 057104, May 2007.
[24] M. Keidar, I. D. Boyd, and I. I. Beilis, "Plasma flow and plasma-wall transition in Hall thruster channel," Phys. Plasmas, vol. 8, pp. 5315–5322, 2001.
[25] J. C. Adam, J. P. Boeuf, N. Dubuit, M. Dudeck, L. Garrigues, D. Gresillon, A. Heron, G. Hagelaar, V. Kulaev, N. Lemoine, S. Mazouffre, J. Perez-Luna, V. Pisarev, S. Tsikata, Physics, simulation, and diagnostics of Hall effect thrusters, Plasma Phys. Control. Fusion, vol. 24, pp. 124041 (2008).
[26] N. B. Meezan and M. A. Cappelli, "Kinetic study of wall collisions in a coaxial Hall discharge," Phys. Rev. E, vol. 66, p. 036401, 2002.
[27] L. Garrigues, G. J. M. Hagelaar, J. Bareilles, C. Boniface, and J. P. Boeuf, "Model study of the influence of the magnetic field configuration and a performance and lifetime of a Hall thruster," Phys. Plasmas, vol. 10, no. 12, pp. 4886–4892, 2003.
[28] Y. Raitses, D. Staack, A. Smirnov, and N. J. Fisch, "Space charge saturated sheath regime and electron temperature saturation in Hall thrusters," Phys. Plasmas, vol. 12, p. 073507, 2005.
[29] Y. Raitses, A. Smirnov, D. Staack, and N. J. Fisch "Measurements of secondary electron emission effects in Hall thrusters", Phys. Plasmas, vol. 13, pp. 014502-2, 2006.
[30] D. Sydorenko, A. Smolyakov, I. Kaganovich, and Y. Raitses, "Modification of electron velocity distribution in bounded plasmas by secondary electron emission," IEEE Trans. Plasma Sci., vol. 34, no. 3, pp. 815–824, Jun. 2006.
[31] D. Sydorenko, A. Smolyakov, I. Kaganovich, and Y. Raitses, "Effects of non-Maxwellian electron velocity distribution function on two-stream instability in low-pressure discharges", Phys. Plasmas vol. 14, pp. 013508, 2007.
[32] D. Sydorenko, I. Kaganovich, Y. Raitses, and A. Smolyakov, "Breakdown of a Space Charge Limited Regime of a Sheath in a Weakly Collisional Plasma Bounded by Walls with Secondary Electron Emission", Phys. Rev. Lett., vol. 103, pp. 145004-4, 2009.
[33] F. Taccogna, R. Schneider, S. Longo, and M. Capitelli, "Modeling of surface-dominated plasmas: From electric thruster to negative ion source," Rev. Sci. Instrum., vol. 79, no. 2, p. 02B 903, 2008.
[34] E. Ahedo and F. I. Parra, "Partial trapping of secondary-electron emission in a Hall thruster plasma," Phys. Plasmas, vol. 12, no. 7, p. 073 503, 2005.
[35] G. D. Hobbs and J. A. Wesson, "Heat flow through a Langmuir sheath in the presence of electron emission," Plasma Phys., vol. 9, no. 1, pp. 85–87, 1967.
[36] H. Bruining "Physics and Application of Secondary Electron Emission", Pergamon Press, London 1954.
[37] Y. Raitses, D. Staack, M. Keidar, and N. J. Fisch, "Electron wall interaction in Hall thrusters," Phys. Plasmas, vol. 12, p. 057104, 2005.
[38] A. Dunaevsky, Y. Raitses, and N. J. Fisch, "Yield of secondary electron emission from ceramic materials of Hall thruster," Phys. Plasmas, vol. 10, pp. 2574–2577, 2003.

[39] L. D. Tsendin, "Energy distribution of electrons in a weakly ionized current-carrying plasma with transverse inhomogeneity," Sov. Phys.JETP, vol. 39, p. 805, 1974.
[40] V.P. Pastukhov. "Classical longitudinal plasma losses from open adiabatic traps." In: Reviews of Plasma Physics, v. 13, p. 203, B.B. Kadomtsev, Ed.(Consultants Bureau, NY, 1987).
[41] D. S. Ryutov , "Axial Electron Heat Loss From Mirror Devices Revisited", Trans. Fusion Sci. Technol., vol.47, pp. 148-154, 2005.
[42] D. Sydorenko, A. Smolyakov, I. Kaganovich, and Y. Raitses, "Plasma-sheath instability in Hall thrusters due to periodic modulation of the energy of secondary electrons in cyclotron motion", Phys. Plasmas, vol. 15, pp. 053506, 2008.
[43] D. Sydorenko, A. Smolyakov, I. Kaganovich, and Y. Raitses, "Kinetic simulation of secondary electron emission effects in Hall thrusters" , Phys. Plasmas, vol. 13, 014501-4, 2006.
[44] A A Ivanov, A A Ivanov Jr, and M Bacal, "Effect of plasma–wall recombination on the conductivity in Hall thrusters", Plasma Phys. Control. Fusion, vol. 44, no. 8, pp. 1463, 2002.
[45] S. Mizoshita, K. Shiraishi, N. Ohno and S. Takamura, "Secondary electron emission from solid surface in an oblique magnetic field", Nucl. Materials, vol. 220-222, pp. 488-492, 1995.
[46] Y. Raitses, J. Ashkenazy G. Appelbaum and M. Guelman, "Experimental Investigation of the Effect of Channel Material on Hall Thruster Characteristics", in Proceedings of the 25th International Electric Propulsion Conference, (Electric Rocket Propulsion Society, Cleveland, OH, 1997), IEPC-97-056, Cleveland, OH, August 1997.
[47] N. Gascon, M. Dudeck, and S. Barral, "Wall material effects in stationary plasma thrusters I: Parametric studies of an SPT-100", Phys. Plasmas, vol. 10, p. 4123, 2003.
[48] Y. Raitses, D. Staack, N. J. Fisch, "Controlling the Plasma Potential Distribution in Segmented Hall Thruster", IEEE Trans. Plasma Sci. vol. 36, no 4, pp. 1202-1203, 2008.
[49] W. Hargus and B. Pote, "Examination of a Hall thruster start transient", AIAA paper-2002-3956, in the proceedings of the 38th Joint Propulsion Conference, Indianapolis, IN, 2002.
[50] Y. Raitses, D. Staack, A. Dunaevsky and N. J. Fisch, "Operation of a segmented Hall thruster with low-sputtering carbon-velvet electrodes", J. Appl. Phys., vol. 99, pp. 036103-3, 2006.
[51] K. D. Diamant, J. E. Pollard, R. B. Cohen, Y. Raitses, and N. J. Fisch, "Segmented Electrode Hall Thruster", Propul. Power, vol. 22, no. 6, pp. 1396-1401, Nov 2006.
[52] J. M. Haas and A. D. Gallimore, "Internal plasma potential profiles in a laboratory-model Hall thruster", Phys. Plasmas vol. 8, 652, 2001; J. A. Linnell, and A. D. Gallimore, "Internal plasma potential measurements of a Hall thruster using xenon and krypton propellant", Phys. Plasmas, vol. 13, 093502, 2006.
[53] D. Staack, Y. Raitses, N.J. Fisch, "Temperature gradient in Hall Thrusters", Applied Physics Letters, 84 (16), 3028-3030 (2004).
[54] D. Staack, Y. Raitses and N. J. Fisch, "Shielded electrostatic probe for nonperturbing plasma measurements in Hall thrusters", Rev. Sci. Instrum., 75 (2), pp. 393-399, (2004).
[55] L. Dorf, Y. Raitses and N. J. Fisch, "Electrostatic Probe Apparatus for Measurements in the Near-Anode Region of Hall Thrusters", Rev. Sci. Instrum., 75 (5),pp. 1255-1260, 2004.
[56] E. Ahedo and D. Escobar, "Influence of design and operation parameters on Hall thruster performances", J. Appl. Phys., vol. 96, pp.983-992, 2004.
[57] M. Cappelli, N. Meezan and N. Gascon, " Transport physics in Hall thrusters, " in Proceedings of the 40th Aerospace Science Meeting, AIAA -2002-0485, Reno, NV, 2002.
[58] M. K. Scharfe, C. A. Thomas, D. B. Scharfe, N. Gascon, M. A. Cappelli and E. Fernandez, "Share-Based Model for Electron Transport in Hybrid Hall Thruster Simulations", IEEE Trans. Plasma Sci., vol. 36, no 5, Oct. 2008.
[59] A. Litvak and N. J. Fisch, "Resistive Instabilities in Hall Current Plasma Discharge," Phys. Plasmas, vol. 8, no 2, pp. 648-651, 2001.
[60] A. M. Kapulkin and V. F. Prisnyakov, Proceedings of the 24th International Electric Propulsion Conference, Moscow, Russia, (Electric Rocket Propulsion Society, Cleveland, OH, 1995), IEPC paper 95-3, Sept. 11–15, 1995.
[61] A. A. Litvak and N. J. Fisch, "Rayleigh Instability in Hall Thrusters", Phys. Plasmas, vol. 11, no. 4, pp. 1379-1381, 2004.
[62] N. J. Fisch, A. Fetterman, Y. Raitses, A. Fruchtman, and J.-M. Rax, Proceedings of the 44th AIAA Joint Propulsion Conference, Hartford, CT, July 2008 (AIAA, Reston, VA, 2009), AIAA paper 2008-4997.

APPENDIX 1. CROSS-SECTIONS FOR ELASTIC ELECTRON-XENON ATOM COLLISIONS USED IN PIC SIMULATIONS

Simulations shown in Fig.3 used EDIPIC code [30] as in our previous simulations [31, 32, 42, 43] but with improved analytical approximations for differential cross sections for elastic scattering. Scattering of electrons in electron-neutral elastic collisions is characterized by the normalized differential cross-section and momentum-transfer collision cross-section in the forms:

$$\frac{\sigma_{sc}(E,\theta)}{\sigma_{sc}(E)} = \frac{1}{4\pi}\frac{1-\xi^2(E)}{[1-\xi(E)\cos\theta]^2}, \qquad \text{(A-1)}$$

$$\frac{\sigma_m(E)}{\sigma_{sc}(E)} = \frac{1-\xi(E)}{2\xi(E)^2}\left((1+\xi(E))\ln\frac{1+\xi(E)}{1-\xi(E)} - 2\xi(E)\right), \qquad \text{(A-2)}$$

where, $\sigma_{sc}\,(E,\,\theta)$ is the differential cross-section, $\sigma_{sc}\,(E)$ is the total cross-section, $\sigma_m\,(E)$ is the momentum-transfer collision cross-section, E is the electron energy in electronvolts, and θ is the angle of scattering relative to the initial direction of electron velocity in the laboratory frame. Here, for elastic scattering of electrons on Xenon atoms at electron energies of $E < 1$kV :

$$\xi(E) = 0.9 + \frac{16.6(\sin(4.8\left|\sqrt{E} - 0.673\right|^{0.43}) - 1.04}{E + 31.4}. \qquad \text{(A-3)}$$

The Princeton Plasma Physics Laboratory is operated
by Princeton University under contract
with the U.S. Department of Energy.

Information Services
Princeton Plasma Physics Laboratory
P.O. Box 451
Princeton, NJ 08543

Phone: 609-243-2245
Fax: 609-243-2751
e-mail: pppl_info@pppl.gov
Internet Address: http://www.pppl.gov